Available online at www.elixirpublishers.com (Elixir International Journal)

Pollution

Elixir Pollution 120 (2018) 51245-51252

ISSN: 2229-712X

Adsorption of Methyl Orange Using Manganese (IV) Oxide Coated Activated Carbon: Kinetic, Thermodynamic and Isotherm Studies.

A.Jimoh and M.B. Ibrahim
Department of Chemistry, Bayero University Kano, Kano State, Nigeria.

ARTICLE INFO

Article history:
Received: 24 May2018;
Received in revised form:
01 July 2018;
Accepted: 11 July 2018;

Keywords:
Methyl Orange,
Activated Carbon,
Nanoparticles,
Kinethic,
Thermodynamic.

ABSTRACT

An activated carbon modified by impregnation with manganese (IV) oxide nanoparticle was prepared and used in for the adsorption of methyl orange (MO) from aqueous solution. Effect of operational parameters such as initial solution pH, contact time, initial dye concentration was studied. The prepared adsorbent shows good adsorption at a wide range of pH (2-10) beyond which adsorption reduces significantly. The maximum adsorption capacity was obtained at 60 min (37.00mg/g). On the thermodynamic point of view, the adsorption process was found to enthalpy-driven. Pseudo-second order kinetic model with Langmuir isotherm model best describe the adsorption process.

Introduction

Dyes and pigments are mostly used in various industries to color the final products. 10–15% of these used dyes released directly into the environment as wastewater. These dyes are toxic, non-biodegradable and apt to cause genetic mutations, and thus have to be removed before discharging into aquatic ecosystems [1,2]. Various traditional treatments methods for dye wastewater treatment such as biological treatment [3], ultrafiltration [4,5], adsorption [6,7] and coagulation–flocculation [8] have been reported in recent years. Among these treatments methods, adsorption has proven to be the most effective conventional process by which the substance is transferred from the liquid phase to the surface of the solid and becomes bound by physical and/or chemical interactions at ambient environment [9]. Due to the excellent adsorption properties, large porous volumes and vast surface areas, porous carbon materials (e.g. activated carbons either modified or unmodified, carbon nanotubes, ordered mesoporous carbons, etc.) have been widely used as adsorbents for wastewater treatment [9–12].

Materials and Methods

Materials: All the chemicals used in the study were of analytical reagent (AR) grade and were used without any further purification. Methyl Orange, MO, (PS Park Scientific Limited). The stock solution of the dye was prepared by taking 1g of methyl orange in 1000mL volumetric flack and subsequent solution were made by serial dilution of this stock solution. During the experiment, the concentration of the dye was determined at 463.2nm using UV-visible spectrophotometer model Hitachi-2800 based on the respective linear calibration curve over desired understudy concentration range. The pH of the solution was adjusted by addition of HCl or NaOH 0.1M using pH/ion meter

Activation of the Neem Leaves

The neem leaves were washed repeatedly with distilled water to remove moisture and impurities. Then the neem leaves were kept in the oven at 90^0C for 3hrs till the leaves turn pale yellow. This was then crushed and screen by 75µm, 300µm and 500µm mesh sizes. The crushed neem leave were mixed with 50% phosphoric acid and heated in a furnace which was initially at room temperature then set to 260^0C for 1h 45min. The sample was removed and allowed to cool in open air. After cooling, the leaves were washed with distilled water severally till the pH reaches 7. Then they were dried in an oven at 110^0C for 45min and then allowed to cool in open air. The cooled sample was then transferred into a sample bottle and labeled AC.

Preparation of Manganese (IV) Oxide Nanoparticle

The manganese (IV) oxide was prepared by hydrothermal process. In the hydrothermal process, $MnCl_2$ (0.18 g) was mixed with isopropanol (50 mL). The $MnCl_2$ solution was then heated to 83°C in a refluxing process for 1hr. 0.10g of $KMnO_4$ was measured and then dissolved in 10mL of deionised water. The $KMnO_4$ solution was added to the refluxed $MnCl_2$ solution. The solution was then allowed to settle and the supernatant was decanted carefully. The remaining solution was centrifuged for 10min and the supernatant discarded. Thus the obtained nanoparticle was washed several times with deionised water. This was followed by drying in oven at 110^0C for 1hr and allowed to cool in open air then transfer into sample bottle labeled MnO_2- NP.

Modification of the Activated Carbon

0.02-0.5g of MnO_2- NP were separately dissolved in 50mL distilled water and 1g of the activated carbon was added to it. The suspensions were mixed by an orbital shaker (250rpm for 3h) at room temperature (30^0C) and filtered. The modified AC was then placed into a furnace at 250^0C for 1h. Finally, the adsorbent was cooled, washed with distilled water (several times), and dried (100^0C for 3h) then transferred into a sample bottle and labeled as AC-MnO_2-NP.

Characterization of the Prepared Adsorbent

The reduction of potassium permanganate to manganese (IV) oxide was monitored by recording UV-Visible spectrum

---

Tele:
E-mail address:jimohabdulmojeed@gmail.com

of the reaction mixture after diluting a small aliquot of the sample with distilled water.Fourier transform infrared (FTIR-Cary 630), Agilent technologies, was used for functional group analysis of the AC-MnO_2-NP over the wave number range of 650–4000 cm−1. The surface morphology of the AC-MnO_2-NP was examined by a scanning electron microscopy (SEM), (Leica Stereoscan-440 interfaced). The concentrations of dye were measured with UV–Vis spectrophotometers (Model Hitachi-2800). The pH measurements were made with Hanna instrument digital pH-meter.

Adsorption Experiments

Batch adsorption experiments were carried out in an incubator shaker at a constant shaking rate (300rpm). The effect of contact time, initial dye concentration, solution pH, adsorbent dose, temperature, and competing ion were studied. 100mL of dye solution of known concentration (10-100mg/L) were shaken in stopped bottles with different weights of adsorbent material (0.1-0.6g) at different temperatures (30-45ºC), for various mixing time (10-120 min) and through the pH range of (2-12) which was adjusted using NaOH or HCl solutions. Separation of the solid phase from liquid was achieved first by centrifuging for 5 min (5000 rpm) followed by filtration. All experiments were carried out in triplicates and the average values were considered. The removal efficiency and adsorption capacity of the adsorbents were calculated by Eq. (1) and (2), respectively:

$$\boldsymbol{R}(\%) = \frac{(C_0 - C_t)}{C_0} \times \mathbf{100} \quad (1)$$

$$q_e = \frac{(C_0 - C_t)V}{m} \quad (2)$$

Where C_0 (mg/L) is the initial dye concentration, C_e (mg/L) is the equilibrium dye concentration, m (g) is the sorbent mass, and V (L) is the volume of the dye solution.

Desorption Study and Reusability Efficiency of the Adsorbent

Desorption studies of AC-MnO_2-NP adsorbed MO dye was carried out using 0.05M H_2SO_4. Desorption of methyl orange from adsorbent surface was carried as follows: after adsorption experiments with methyl orange under optimum conditions, the AC-MnO_2-NP was separated and washed with 0.05M H_2SO_4 to remove adsorbed methyl orange. The regenerated adsorbent was then reused for adsorption processes. The adsorption–desorption procedure was repeated five times, each times with fresh solution. At every adsorption-desorption process, the colour intensity of the desorbed methyl orange was measured at 463.2nm.

$$\textit{Percentage desorption} = \frac{\textit{amount of dye liberated by acid}}{\textit{amount of dye adsorbed on adsorbent}}\ x\ 100 \quad (3)$$

$$\textit{Reusability efficiency} = \frac{\textit{amount of dye adsorbed by regenerat edadsorbent}}{\textit{amount of dye adsorbed by fresh adsorbent}}\ x\ 100 \quad (4)$$

Results and Discussion

UV-Visible Studies of Manganese (IV) Oxide Nanoparticles

UV-Visible absorbance spectroscopy has proved to be a very useful technique for studying metal nanoparticles because the peak positions and shapes are sensitive to particle size. Figure 4.1 shows UV-Visible spectra of manganese oxide nanoparticles synthesized by hydrothermal process as a function of wavelength. The characterization of manganese (IV) oxide nanoparticles by UV-spectrophotometer was carried out from the range 200 to 800nm. The UV-visible absorption shows sharp absorption at 355.0 nm due to manganese oxide nanoparticles. Kumar *et al.* (2013) synthesis MnO_2 nanoparticles using co-precipitation method and during the characterization they observed a similar value of 339.60 nm. Butterfield *et al.* (2013) obtained a value of 360.0 nm in their study of Mn (II,III) oxidation and MnO_2mineralization by an expressed bacterial multicopper oxidase

Fig 1. UV-Vis spectra of manganese (IV) oxide nanoparticles.

Fourier Transform- Infrared (FT-IR) Characterization

FT-IR spectroscopy was used to investigate the interactions between different species and changes in chemical compositions of the adsorbents (AC-MnO_2-NP) before and after adsorption of the dye. Figure 2 presents FTIR spectrum of the adsorbent before and after adsorption of methyl orange while Table 1 presents peaks and frequencies of IR adsorption as well as associated functional groups.

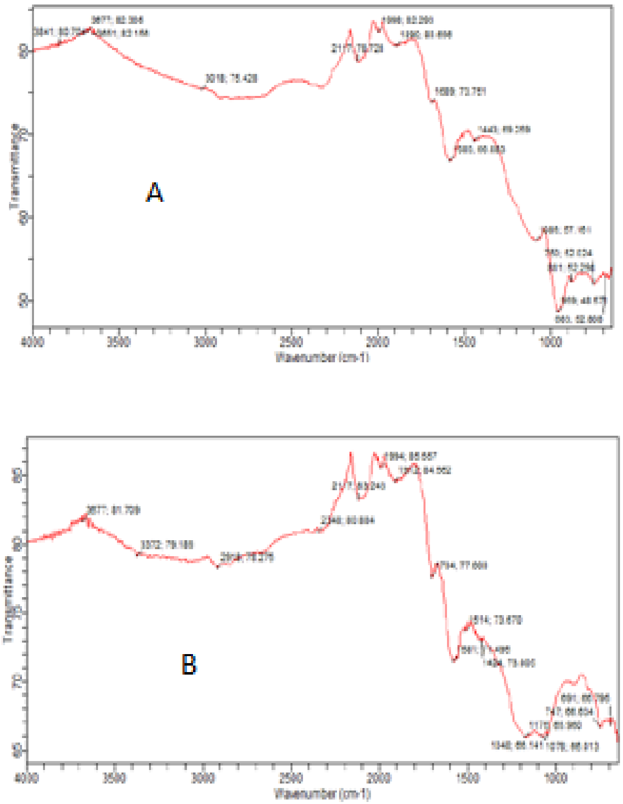

Fig 2. FTIR spectra of (A) AC-MnO_2-NP and (B) MO loaded AC-MnO_2-NP.

The vibrational energy associated with the adsorbents can be determined using Equation 4 is used, also Equation 5 gives the vibrational energy difference, after adsorption of the dye by the adsorbents.

$$\mathbf{E = hc\bar{\upsilon}} \quad (5)$$

$$\mathbf{\Delta E = E_{after\ adsorption} - E_{before\ adsorption}} \quad (6)$$

Where h is Planck's constant (6.626 x 10^{-34} m^2Kg/s), c is the speed of light (3.0 x 10^8 m/s), and $\bar{\upsilon}$ is the wave number (cm^{-1}) of the reference peak. Tables 2 show the values of the vibrational energy difference after adsorption of MO by the AC-MnO_2-NP. As observed from the table, in most case, there is an increase in vibrational energy. This may be due to the anionic nature of methyl orange

Table 1. FTIR Peak, Frequency and Assignment of AC-MnO_2-NP before and after adsorption.

Before Adsorption		After Adsorption		
Peak	**Intensity**	**Peak**	**Intensity**	**Assignment**
3018	75.428	3398	80.497	O-H stretching vibration in carboxylic acid groups (2500-3500cm^{-1})
2117	78.728	2113	83.560	O-H stretching vibration in carboxylic acid groups (2500-3500cm^{-1})
1689	73.751	1704	77.916	General presence of C=O groups stretching vibrations (1650-1800cm^{-1})
1585	66.883	1599	71.247	C-H bending due to alkene
1443	69.259	1443	73.044	OH in carboxylic acid groups due to in-plane OH bending (1440-1400cm^{-1})
1088	57.161	1115	66.215	C-N stretching vibration in amines (1030-1330cm^{-1})
683	52.808	750	65.980	O-C=O in carboxylic acid groups due to O-C=O bending (700-590cm-1); C-C-CHO inaldehyde compounds due to C-C-CHO bending (695-635cm^{-1})

Table 2. Vibrational Energy Difference of Some Peaks before and after Adsorption of MO by the AC-MnO_2-NP.

Before Adsorption		After Adsorption (MO-Loaded)		
Peak	**E(J)**	**Peak**	**E (J)**	**ΔE (J)**
3018	5.9991 $x10^{-24}$	3372	6.7028 $x10^{-24}$	0.7037 $x10^{-24}$
2117	4.2081 $x10^{-24}$	2113	4.2002$x10^{-24}$	-0.0079 $x10^{-24}$
1585	3.1506 $x10^{-24}$	1599	3.1784$x10^{-24}$	0.0278 $x10^{-24}$
1088	2.1627 $x10^{-24}$	1115	2.2163$x10^{-24}$	0.0536 $x10^{-24}$
683	1.3576 $x10^{-24}$	750	1.4908$x10^{-24}$	0.1332 x 10^{-24}

Scanning Electron Microscopy (SEM)

Scanning Electron Microscopy studies provide useful information regarding the surface morphology of the adsorbents. Generally the adsorbent with porous and rough morphology has high adsorption capacity [13]. The SEM images of AC-MnO_2-NP before and after adsorption are presented in Figures 3. It can be seen that the SEM of AC-MnO_2-NP mixture shows a flake clustered particle which are irregular in shape and also revealed the surface texture and porosity nature. From these micrographs and pores structures are evidence on the surface of the prepared adsorbent. The images show that the adsorbent is rough and uneven. Pores that are present on the adsorbent surface reduce resistance to adsorbed molecules and thus facilitate their diffusion from the aqueous solution onto the adsorbent surface. A significant pore structure exists with a series of rocky structure distributed over the surface of dye loaded AC-MnO_2-NP.

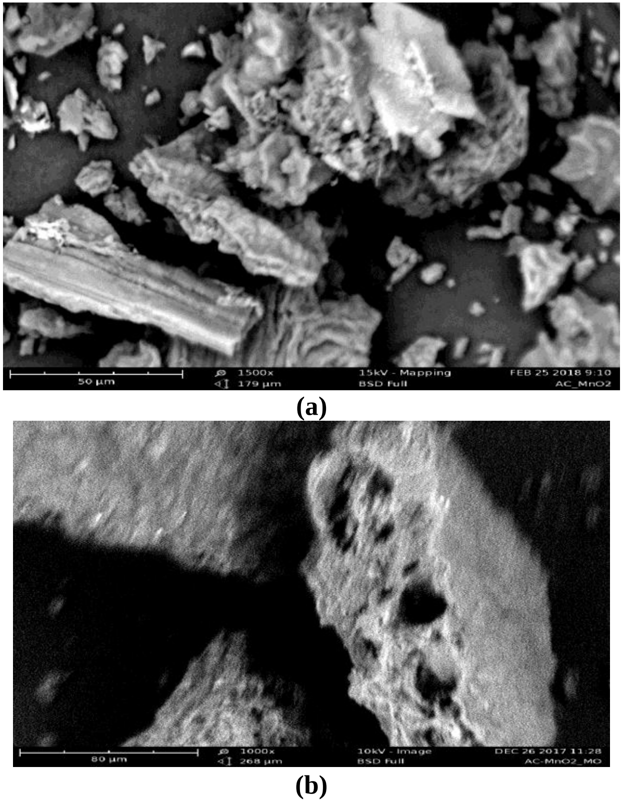

(a)

(b)

Fig 3. SEM image of (A) AC-MnO_2-NP (B) MO loaded AC-MnO_2-NP.

Effect of pH

The pH value of methyl orange solution plays an important role in the whole adsorption process, influencing not only the surface charge of the adsorbent, and the dissociation of functional groups on the active sites of the adsorbent, but also the chemistry of MO solution [14]. Generally, the pH of the adsorption depends on the zero point charge of the methyl orange (pHzpc) and the charge of the adsorbent surface [15]. The structure of methyl orange is dependent on the solution pH. As the pH of the solution is increased to more basic conditions, the double bond conjugation in the structure is lost and a proton is lost, and the molecule rearranges to form a negatively charged species as shown in figure 4. The positive charges have been neutralized. Due to excess anions in the solution, there will be repulsion of the dye by the negatively charged surfaces of the adsorbents [16].

The effect of pH value of initial methyl orange solutions on adsorption is shown in Fig. 4. As it can be observed from the Figure, there was a gradual decrease in adsorption capacity of the adsorbent when the pH value of MO solutions varied from 2 to 10. Adsorption capacity decreased significantly at pH value higher than 10. These results indicated that this adsorbent has shown a relatively stable removal toward methyl orange in a wide range of pH (2 – 10). According to the literatures [17, 18, 19] the optimum pH was frequently reported to be around pH 2–7 when modified activated carbon was used as adsorbent. In this study, a great adsorption was observed in a wide pH range of 2–10.

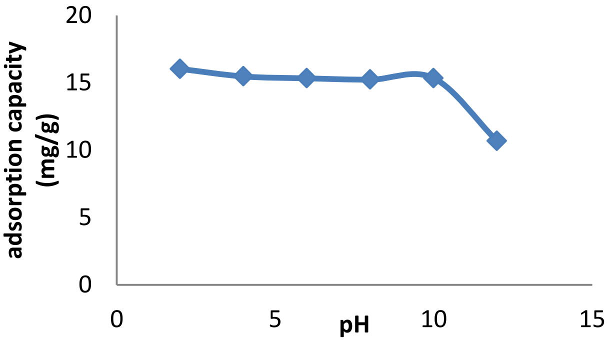

Fig 4. Effect of pH on the adsorption of methyl orange by AC-MnO_2-NP.

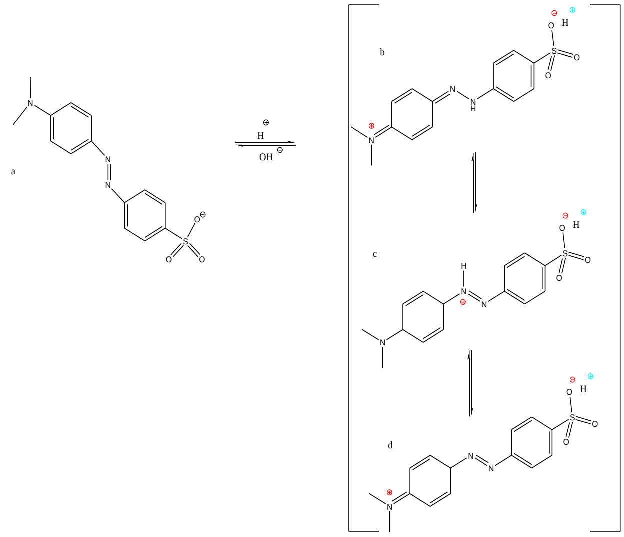

Fig 5. Alkaline form of Methyl orange (a) and its mono-protonated zwitter ionic structures under acidic conditions (b, c and d).

Effect of contact time

The adsorption capacity of AC-MnO$_2$-NP for the removal of methyl orange at 40mgL^{-1} at various contact time (0 – 120min) was investigate (Fig. 6). The maximum adsorption was 37.00mg/g at a time of 60min. The steep and high initial adsorption rate at a time of 0 – 10min slowly changes as the time progresses. This observation may be due to high ratio of vacant surface site to adsorbate molecule at this initial period. Similar result was observed by Ghaedi *et al.*, in their adsorption studies of methyl orange and sunset yellow using gold nanoparticle loaded on activated carbon [17].

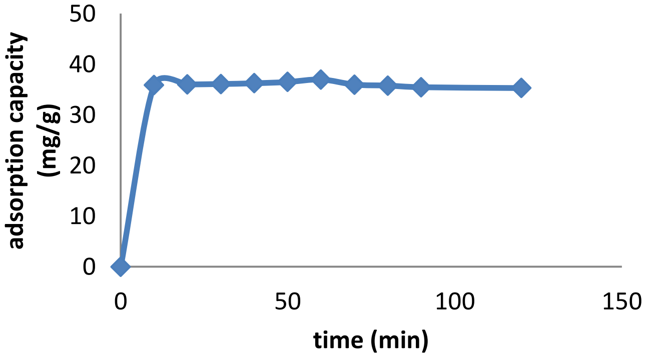

Fig 6. Effect of contact time on the adsorption of methyl orange by AC-MnO$_2$-NP.

Effect of Initial Adsorbate Concentration

A given mass of sorbent material can only adsorb a fixed amount of dye. Hence, the initial dye concentration of an effluent is one of important factor to study. The effect of increment in dye initial concentration will increase the adsorbent loading capacity. The effect of initial dye concentration on the adsorption of methyl orange from aqueous solution by AC-MnO$_2$-NP was studied by varying initial methyl orange concentration range of 10–100 mg/L at adsorbent dose of 0.1g at 303 K and it is represented in Fig 7. As seen from the Figure, the adsorption of the adsorbate from aqueous solution by AC-MnO$_2$-NP was found to increase with increasing in initial dye concentration. The increase in the adsorption capacity of the dye adsorbed with an increase in the initial adsorbate concentration is due to increase in mass transfer driving force resulting from concentration gradient developed between the bulk solution and surface of the adsorbent [33].

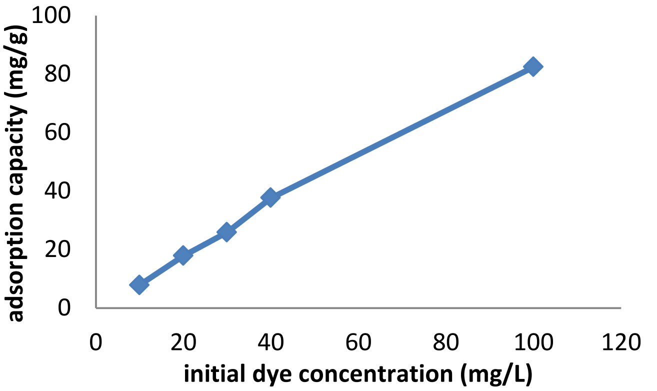

Fig 7. Effect of initial dye concentration on the adsorption of methyl orange by AC-MnO$_2$-NP.

Kinetic of the adsorption process

Lagergren Pseudo First Order Model

Lagergren Pseudo first-order (PFO) rate equation is the earliest known model describing the adsorption rate based on the adsorption capacity [20]. The equation representing this model is:

$$\log(q_e - q_t) = \log q_e - \frac{k_1}{2.303}t \qquad (7)$$

Where k_1 is the pseudo first order rate constant in g/mg min q_e is the amount adsorbed at equilibrium q_t is the amount adsorbed at time t and t is the time. A plot of log (q_e – q_t) against t (graph not shown) will give a slop equal to k_1 and intercept of q_e. The calculated q_e, k_1, and the corresponding linear regression correlation coefficient R^2 values are shown in Table 1.

Lagergren Pseudo Second Order Model

Pseudo-second-order (PSO) rate expression is mostly used in an attempt to describe adsorption process. It has been widely applied to the adsorption of pollutants from aqueous solutions. This model is represented by the equation.

$$\frac{dq_t}{dt} = k_2(q_e - q_t)^2 \qquad (8)$$

The linear form of the equation is given by

$$\frac{t}{q_t} = \frac{1}{k_2 q_e^2} + \frac{1}{q_e}t \qquad (9)$$

Where k_2 is the pseudo first order rate constant in mol/g min, q_e is the amount adsorbed at equilibrium,

q_t is the amount adsorbed at time t and t is the adsorption time. A plot of $\frac{t}{q_t}$ against t graph not shown give a straight line graph with slop of $\frac{1}{q_e}$ and intercept of $\frac{1}{k_2 q_e^2}$. The calculated q_e, k_2, and the corresponding linear regression correlation coefficient R^2 values are summarized in Table 1.

The Elovich equation

The Elovich equation is simply expressed as:

$$\frac{dq_t}{dt} = \propto e^{-\beta q_t} \qquad (10)$$

The linear form of Elovich equation is

$$q_t = \frac{1}{\beta}\ln(\alpha\beta) + \frac{1}{\beta}\ln t \qquad (11)$$

Where α is the initial desorption rate (mg/(g min)) and β is the desorption constant (g/mg) during any experiments. A plot of q_t against lnt (graph not shown) gives a slope and intercept of $\frac{1}{\beta}$ and $\frac{1}{\beta}\ln(\alpha\beta)$ respectively. The best-fit values of k_1, k_2, α, and β along with coefficient of determination (R^2) for the PFO, PSO and Elovich models for MO adsorption onto AC-MnO$_2$-NP with C_o(MO) = 100 mg/L at 303 K with m = 0.1g of adsorbent are given in Table 3.

According to the results, PSO kinetic model has the highest R^2 values and also the value of $q_{e,cal}$ (38.46 mg/g) is much closer to $q_{e,exp.}$ (37.00 mg/g). Therefore, the adsorption of the adsorbate is best described by the PSO kinetic model.

Table 3. Kinetic parameters for the removal of MO from aqueous solution onto AC-MnO$_2$-NP (C$_o$ = 40 mg/L, m = 0.1 g, T = 303 K).

Model	Kinetic parameter	Values
	$q_{e,exp.}$(mg/g)	37.00
PFO	$q_{e,cal.}$(mg/g)	1.045
	k_1(min^{-1})	0.044
	R^2	0.716
PSO	$q_{e,cal.}$(mg/g)	38.46
	k_2(g/mg.min)	0.017
	R^2	0.997
Elovich	α(mg/g.min)	1.13x10^{10}
	β(mg/g)	0.739
	R^2	0.363

Adsorption isotherms

The equilibrium adsorption isotherm can be obtained by plotting the concentration at the surface of a solid phase versus the concentration in the liquid phase. The distribution of the adsorbate between the sorbent and the liquid phase is a measure of the position of equilibrium in the adsorption process and can generally be expressed by isotherm models [14]. In the present investigation, the equilibrium data were analyzed according to Langmuir, Freundlich, temkin and Dubinin-Radushkevich isotherm model.

Langmuir Isotherm

Langmuir adsorption which was primarily designed to describe gas-solid phase adsorption is also used to quantify and contrast the adsorptive capacity of various adsorbents [21]. Langmuir isotherm takes into accounts the surface coverage by balancing the relative rates of adsorption and desorption (dynamic equilibrium). Adsorption is proportional to the fraction of the surface of the adsorbent that is open while desorption is proportional to the fraction of the adsorbent surface that is covered [22]. The linear form of Langmuir Equation is shown in Equation 12:

$$\frac{c_e}{q_e} = \frac{1}{q_m k_L} + \frac{c_e}{q_m} \quad (12)$$

Where C_e is concentration of adsorbate at equilibrium (mg g−1), K_L is Langmuir constant related to adsorption capacity (mg g−1), which can be correlated with the variation of the suitable area and porosity of the adsorbent which implies that large surface area and pore volume will result in higher adsorption capacity [24].

The essential characteristics of the Langmuir isotherm can be expressed by a dimensionless constant called the separation factor R_L.

$$R_L = \frac{1}{1+K_L c_0} \quad (13)$$

Where K_L is Langmuir constant (mg g^{-1}) and c_0 is initial concentration of adsorbate (mg g^{-1}). R_L values indicate the adsorption to be unfavourable when $R_L > 1$, linear when $R_L = 1$, favourable when $0 < R_L < 1$, and irreversible when $R_L = 0$ [24].

As seen from tables 4, the goodness of fit values, (R^2) for Langmuir is closer to unity in comparison to values obtained for the other three isotherms. This showed an evidence that the adsorption follows the Langmuir isotherm indicating the existence of identical adsorption site with monolayer adsorption predominating. The R_L value obtained is lower than 1 proposed that adsorption of the dyes onto the adsorbents was a favourable process and as seen in Table 5, increasing initial dye concentrations caused R_L values to gained closer to zero value, meaning higher adsorbate concentrations were more appropriate for favourable methyl orange adsorption [36].

Freundlich Isotherm

Freundlich isotherm is applicable to adsorption processes that occur on heterogonous surfaces [23]. This isotherm gives an expression which defines the surface heterogeneity and the exponential distribution of active sites and their energies [24]. The linear form of the Freundlich isotherm is as follows:

$$\boldsymbol{lnq_e = lnK_F - \frac{1}{n} lnC_e} \quad (14)$$

Where K_F is adsorption capacity (L/mg) and 1/n is adsorption intensity; it also indicates the relative distribution of the energy and the heterogeneity of the adsorbate sites.

As seen in table 4, the value of 1/n is less than unity, which is an indication of a unilayer adsorption process, and not a cooperative adsorption, where the 1/n value will be above unity [25]. Also, since 1/n is less than unity, the adsorption of dyes by the adsorbent is a physical process involving adsorbate–adsorbent interactions.

Temkin Isotherm

Temkin isotherm model takes into account the effects of indirect adsorbate/adsorbate interactions on the adsorption process; it is also assumed that the heat of adsorption (ΔHads) of all molecules in the layer decreases linearly as a result of increase surface coverage [26]. The Temkin isotherm is valid only for an intermediate range of ion concentrations [27]. The linear form of Temkin isotherm is given below:

$$\boldsymbol{q_e = B_T lnK_T + B_T lnC_e} \quad (15)$$

$$\boldsymbol{B_T = \frac{RT}{b_T}} \quad (16)$$

T is the absolute temperature in kelvin, R is the universal gas constant (8.314Jmol^{-1}K^{-1}), and B_T is related to heat of adsorption, while K_T is the equilibrium binding constant (Lmg^{-1}). A plot of q_e against lnC_e (not shown) gives a slop and intercept of B_T and $B_T$lnK_T respectively.

As seen in table 4, according to the results, adsorbates adsorption on this modified adsorbent has higher exothermic value (0.216 kJ/mol), thus suggesting that most favorable interaction occurs with this adsorbent from the thermodynamic point of view. However, the value of these energy factors seem relatively low, which can be ascribed to the fact that the adsorption process deals with hydrophobic interactions which do not release energy compared to polar or ionic interactions, which is mainly due to dehydration/hydration behaviour [13]. Also, the value of this energy factor less than 8kj/mol, shows the sorption process is physical in nature and this is supported by the results of Freundlich isotherm modeling. In addition, good linear regression value (0.957), indicates that adsorption process is fit with Temkin isotherm model.

Dubinin-Radushkevich Isotherm

Dubinin-Radushkevich Isotherm model is an empirical adsorption model that is generally applied to express adsorption mechanism with Gaussian energy distribution onto heterogeneous surfaces [28]. This isotherm is also suitable for intermediate range of adsorbate concentrations because it exhibits unrealistic asymptotic behavior and does not predict Henry's laws at low pressure [29].

Dubinin-Radushkevich model is a semi-empirical equation in which adsorption process follows a pore filling mechanism [30]. This model presumes a multilayer character involving Van Der Waal's forces, applicable for physical adsorption processes, and it is also a fundamental equation that qualitatively describes the adsorption of gases and vapours on microporous sorbents [31]. It is mostly applied to differentiate between physical and chemical adsorption [30].

A distinguishing feature of the Dubinin-Radushkevich isotherm model is the fact that it is temperature dependent; hence when adsorption data at different temperatures are plotted as a function of logarithm of amount adsorbed versus the square of potential energy, all suitable data can be obtained [22].

The well-known linear expression of D-R isotherm model is demonstrated in Equation 16, where q_e: Amount of dye adsorbed at equilibrium (mg/g), K_{DR}: D-R isotherm constant (mol^2/kJ^2) associated with mean free adsorption energy of adsorbate molecules per mole as they are transferred from solution media onto the adsorbent surface. q_{max}: Theoretical isotherm saturation capacity (mg/g), ε: Polanyi potential (J/mol). Expression of Polanyi potential is also given in Equation 17. The D-R plot of $\ln q_e$ versus ε^2 (not shown) gives the slope which is equivalent to the isotherm constant, K_{DR}, and the intercept equivalent to the maximum adsorption capacity, $\ln q_{max}$.

$$\boldsymbol{\ln q_e = K_{DR}\varepsilon^2 + \ln q_{max}} \qquad (17)$$

$$\boldsymbol{\varepsilon = RT\ln(1 + {}^{1}/_{C_e})} \qquad (18)$$

The E values specify the type of adsorption process. The chemical ion exchange happened for the E value 8-16 kJ/mol. The physical and chemical adsorptions occurred when E < 8 and E > 8 kJ/mol, respectively [32]. As shown in table 2, the E values for the adsorption of the dye is 1.581 kJ/mol. This shows that the adsorption of the dye by either of the adsorbent was defined as physical in nature. This is also supported by Freudlish and Temkin isotherm model.

Table 4. Isotherms parameter for adsorption of methyl orange AC-MnO$_2$-NP.

Isotherm	**Parameters**	**Value**
Langmuir	R^2	0.997
	q_0 (mg g^{-1})	66.667
	b (L mg^{-1})	0.263
	R_L	0.169
Fraundlich	R^2	0.944
	1/n	0.409
	K_F (mg g^{-1})	15.059
Temkin	R^2	0.991
	B_T (mg L^{-1})	11.63
	b_T (kJ mol^{-1}/ (mg L^{-1}))	0.216
	K_T (L mg^{-1})	4.146
Dubinin and Radushkevich	R^2	0.836
	B (mol^2 J^{-2})	2 x 10^{-7}
	q_D (mg g^{-1})	44.478
	E (kJ mol^{-1})	1.581

Table 5. R_L values for adsorption of methyl orange on the AC-MnO$_2$-NP.

Concentration	R_L Values
10	0.3717
20	0.2283
40	0.1289
60	0.0897
80	0.0689
100	0.0559

Adsorption Thermodynamic

In the evaluation of the present adsorption process, certain thermodynamic factors were computed, because the thermodynamic functions contribute essentially in understanding the nature of adsorption. The thermodynamic parameters which are related generally to the adsorption of dyes, such as, enthalpy change ΔH_{ads} (kJ/mol), entropy change ΔS_{ads} (kJ/ mol. K) and Gibbs free energy change ΔG_{ads} (kJ/mol) have been calculated according to the following expressions:

$$\mathbf{Kc} = \frac{\mathbf{Q_e}}{\mathbf{C_e}} \qquad (19)$$

$$\Delta G_{ads} = \Delta H_{ads} - T\,\Delta S_{ads} \qquad (20)$$

$$\mathbf{\ln Kp = -\Delta H_{ads}/RT + \Delta S_{ads}/R} \qquad (21)$$

Where K_p is the thermodynamic equilibrium constant, i.e., the ratio of the equilibrium concentration of the adsorbate (methyl orange) on the adsorbent (AC-MnO$_2$-NP) (Q_e) to that in solution (C_e). T is the absolute temperature in Kelvin, and R is the universal gas constant (8.314 J/mol. K). The Plotting of $\ln K_c$ against 1/T give a slope and intercept equal to $-\Delta H_{ads}/R$ and $\Delta S_{ads}/R$, respectively (Fig. 8). As seen from the Figure, K_c values increases with increasing temperatures and that means the mobility of methyl orange decreases with gradual increase in adsorption temperature, referring that interactions between adsorbent and adsorbate molecules were getting stronger and amount of adsorbed methyl orange were increased [34].

As observed in Table 6, the negative values of ΔH_{ads} for the adsorption of methyl orange by the adsorbent revealed that the adsorption process is exothermic in nature. Adsorption in the liquid phase is a complex phenomenon in which the solute and the solvent compete for the solid surface. Adsorption and desorption of the solute and the solvent molecules take place simultaneously, and the adsorption process involves energy changes that could result in either a positive or negative ΔH_{ads} [35]. Also the adsorption of the adsorbates from aqueous solution is feasible and spontaneous at all the temperatures investigated as indicated from the negative values of ΔG_{ads}. The decrease in the absolute value of ΔG_{ads}, shows that spontaneity of the process decreases with increase in temperature [36]. Considering Eq. 14, if the absolute value of ΔH is greater than the absolute value of TΔS (/ΔH/ > /TΔS/), this means that the flow of thermal energy provide most of the free energy in the adsorption process. While if /ΔH/ < /TΔS/, this shows that increasing disorder provide most of the process free energy. As seen in Table 6, /ΔH/ > /TΔS/ at all temperature studied, this shows that the adsorption process is enthalpy-driven.

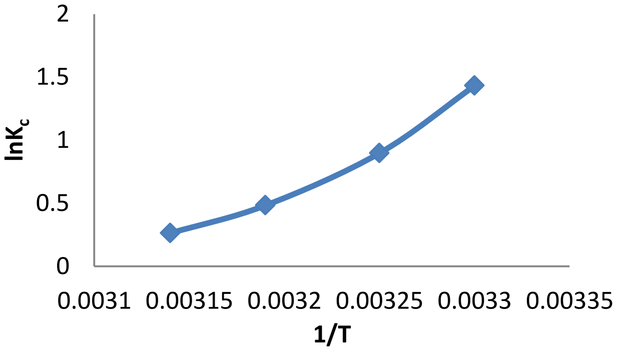

Fig. 8. Van't Hoff plot for adsorption of methyl orange onto AC-MnO$_2$-NP.

Table 6a. Thermodynamic parameters for the adsorption of MO onto the AC-MnO$_2$-NP (C_o = 100 mg/L, m = 0.6 g).

ΔH_{ads} (kJ/mol)	**ΔS_{ads} (kJ/molK)**	**ΔG_{ads} (kJ/mol) $\Delta G_{ads} = \Delta H_{ads} - T\,\Delta S_{ads}$**			
		303	308	313	318
-60.260	-0.187	-3.599	-2.664	-1.729	-0.794

Table 6b. Dependency of ΔG to ΔH and TΔS for adsorption of MO by the adsorbent.

/ΔH/	**/TΔS/**			
	303	308	313	318
60.260	56.661	57.596	58.531	59.466

Desorption Study and Reusability efficiency of the adsorbent

Desorption studies help to elucidate the nature of adsorption and to recover the valuable methyl orange from aqueous solution using the adsorbent. Attempts were made to the effective desorption of methyl orange from the spent AC-MnO_2-NP using 0.05M H_2SO_4. The reusability efficiency of the adsorbent and percentage desorption of adsorbate is shown in Figure 9.

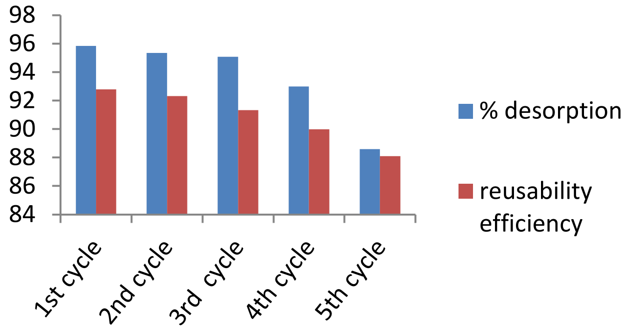

Fig. 9. Reusability efficient of Ac-MnO_2-NP and percentage desorption of methyl orange.

Reference

[1] L. Donnaperna, L. Duclaux, R. Gadiou, M.P. Hirn, C. Merli, L. Pietrelli, "Comparison of adsorption of Remazol Black B and Acidol Red on microporous activated carbon felt" J. Colloid Interface Sci. vol. 339 pp. 275–284, 2009.

[2] C. Tizaoui, and N. Grima, "Adsorption of aromatic compounds by carbonaceous adsorbents: a comparative study on granular activated carbon, activated carbonfiber and carbon nanotubes" Environ. Sci. Technol. Vol. 44 pp. 6377–6383, 2010.

[3] M. Kornaros, and G. Lyberatos, "Biological treatment of wastewaters from a dye manufacturing company using a trickling filter" J. Hazard. Mater. Vol. 136 pp. 95–102, 2006.

[4] A.L. Ahmada, S.W. Puasab, M.M.D. "Zulkali, Micellar-enhanced ultrafiltration for removal of reactive dyes from an aqueous solution" Desalination. Vol. 191 pp. 153–161, 2006

[5] F. Banat, N.A. Bastaki, "Treating dye wastewater by an integrated process of adsorption using activated carbon and ultrafiltration" Desalination. Vol. 170 pp. 69–75, 2004.

[6] E. Haque, J.W. Jun, S.H. Jhung, "Adsorptive removal of methyl orange and methylene blue from aqueous solution with a metal-organic framework material, iron terephthalate (MOF-235)", J. Hazard. Mater. Vol. 185 pp. 507–511, 2011.

[7] K.P. Singh, D. Mohan, S. Sinha, "Color removal from wastewater using low-cost activated carbon derived from agricultural waste material" Ind. Eng. Chem. Res. Vol. 42 pp. 1965–1976, 2003.

[8] A. Szygu1a, E. Guibal, M.A. Palacın, "Removal of an anionic dye (Acid Blue 92) by coagulation–flocculation using chitosan" J. Environ. Manage. Vol. 90 pp. 2979–2986, 2009.

[9] L.R. Roberto, O.P. Raul, M.B. Jovita, External mass transfer and hindered diffusion of organic compounds in the adsorption on activated carbon cloth, Chem. Eng. J. vol. 183 pp. 141–151, 2012

[10] X. Zhuang, Y. Wan, C.M. Feng, Y. Shen, D.Y. Zhao, "Highly efficient adsorption of bulky dye molecules in wastewater on ordered mesoporous carbons" Chem. Mater. Vol. 21 pp. 706–716, 2009.

[11] S. Altenor, B. Carene, E. Emmanuel, J. Lambert, J.J. Ehrhardt, S. Gaspard, "Adsorption studies of methylene blue and phenol onto vetiver roots activated carbon prepared by chemical activation" J. Hazard. Mater. Vol. 165 pp. 1029–1039, 2009.

[12] L.L.Ji,Y.Shao,Z.Y.Xu,S.R.Zheng,D.Q. Zhu, "Adsorption of monoaromatic compounds and pharmaceutical antibiotics on carbon nanotubes activated by KOH etching" Environ. Sci. Technol. Vol. 44 pp. 6429–6436, 2010.

[13] A.A.Olajire, J.J.Abidemi, A. Lateef, and N.U. Benson,"Adsorptive Desulphurization of Model Oil by Ag Nanoparticle-Modified Activated Carbon Prepared from Brewer's Spent Grains" Journal of Environmental Chemical Engineering. Vol. 5 pp. 147-159, 2017

[14] H. Ruihua, L. Qian, H. Jie, and Y.Bingchao"Adsorption of methyl orange onto protonated crosslinked chitosan"Arabian Journal of Chemistry.Vol. 10 pp. 24–32, 2017.

[15] J. Tang, Z.F. Yang, and Y.J. Yi, "Enhanced Adsorption of Methyl Orange by Vermiculite Modified by Cetyltrimethylammonium Bromide (CTMAB)"Procedia Environmental Sciencesvol. 13 pp. 2179 – 2187, 2002.

[16] Fortunate Phenyo Sejie and Misael Silas Nadiye-Tabbiruka "Removal of Methyl Orange (MO) from Water by adsorption onto Modified Local Clay (Kaolinite)"Physical Chemistry.Vol. 6 no. 2 pp. 39-48, 2016. DOI: 10.5923/j.pc.20160602.02

[17] M. Ghaedi, F. Mohammgi, and A. Ansari, "Gold nanoparticle loaded on activated carbon as novel adsorbent for kinetic and isotherm and isotherm studies of methyl orange and sunset yellow adsorption", Journal of Dispersion Science and Technology vol. 36 no. 5 pp. 652-659, 2015.

[18] P. Jolly, K.D. Manas, and K.D.D.Dhananjay "Verma Removal of methyl orange by activated carbon modified by silver nanoparticles". Appl. Water Sci.vol. 3 pp. 367–374, 2013 DOI 10.1007/s13201-013-0087-0

[19] M.N. Rashed, M.A.Eltaher, and A.N.A. Abdou, "Adsorption and photocatalysis for methyl orange and Cd removal from wastewater using TiO2/sewage sludge-based activated carbon nanocomposites". R. Soc. open sci.vol. 4pp. 170834, 2017, http://dx.doi.org/10.1098/rsos.170834

[20] Y.S. Ho, "Review of second order models for adsorption systems". hazadous material, vol. B136 pp. 681-689, 2006.

[21] T. M. Elmorsi, "Equilibrium isotherms and kinetic studies of removal of methylene blue dye by adsorption onto miswak leaves as a natural adsorbent," Journal of Environmental Protection, vol. 2 no. 6 pp. 817–82, 2011.

[22] A. G¨unay, E. Arslankaya, and I. Tosun, "Lead removal from aqueous solution by natural and pretreated clinoptilolite: adsorption equilibrium and kinetics," *Journal* of Hazardous Materials, vol. 146, no. 1-2, pp. 362–371, 2007.

[23] N. Ayawei, S. S. Angaye, D. Wankasi, and E. D. Dikio, "Synthesis, characterization and application of Mg/Al layered double hydroxide for the degradation of congo red in aqueous solution," Open Journal of Physical Chemistry, vol. 5, no. 03, pp. 56–70, 2015.

[24] N. Ayawei, A.N. Ebelegi, and D. Wankasi, "Modelling and Interpretation of Adsorption Isotherms" Journal of Chemistry, Vol. 2017, Article ID 3039817, 11 pages, August 2017. doi.org/10.1155/2017/3039817

[25] Farhan A.M., Al-Dujaili H.A., and Awwad M.A., (2013) Equilibrium and kinetic studies of cadmium (II) and lead (II) ions biosorption onto Ficus carcia leaves, *Int. J. Ind. Chem.* 4: 24–31.

[26] D. Ringot, B. Lerzy, K. Chaplain, J.-P. Bonhoure, E. Auclair, and Y. Larondelle, "In vitro biosorption of ochratoxin A on the yeast industry by-products: comparison of isotherm models," *Bioresource Technology*, vol. 98, no. 9, pp. 1812–1821, 2007.

[27] H.Shahbeig,N.Bagheri, S. A. Ghorbanian, A. Hallajisani, and S. Poorkarimi, “A new adsorption isotherm model of aqueous solutions on granular activated carbon,” *World Journal of Modelling and Simulation*, vol. 9, no. 4, pp. 243–254, 2013.

[28] O. C¸elebi, C¸. ¨ Uz¨um, T. Shahwan, and H. N. Erten, “A radiotracer study of the adsorption behavior of aqueous Ba2+ ions on nanoparticles of zero-valent iron,” *Journal of Hazardous Materials*, vol. 148, no. 3, pp. 761–767, 2007.

[29] C. Theivarasu and S. Mylsamy, “Removal of malachite green from aqueous solution by activated carbon developed from cocoa (Theobroma Cacao) shell—A kinetic and equilibrium studies,” *E-Journal of Chemistry*, vol. 8, no. 1, pp. S363–S371, 2011.

[30] K. Vijayaraghavan, T. V. N. Padmesh, K. Palanivelu, and M. Velan, “Biosorption of nickel(II) ions onto Sargassum wightii: application of two-parameter and three-parameter isotherm models,” *Journal of Hazardous Materials*, vol. 133, no. 1–3, pp. 304–308, 2006.

[31] U. Israel and U. M. Eduok, “Biosorption of zinc from aqueous solution using coconut (Cocos nuciferaL) coirdust,” *Archives of Applied Science Research*, vol. 4, pp. 809–819, 2012.

[32] Nourmoradi H, Khiadani M, and Nikaeen M. (2013). Multi-component Adsorption of Benzene, Toluene, Ethylbenzene, and Xylene from Aqueous Solution by Montmorillonite Modified with Tetradecyl Trimethyl Ammonium Bromide, *J. Chem. 2013*. 1-10

[33] Anbia, M. and Parvin, Z. (2011). Desulphurization of fuel by means of nanoporous carbon adsorbent, *Chem. Eng. Res. Dev*. 89:641–647.

[34] Lian L, Guo L, and Guo C. (2009). Adsorption of Congo red from aqueous solutions onto Ca-bentonite. *J Hazard Mater*. 161(1):126–31.

[35] Kumar, M. and Tamilarasan, R. (2013). Modeling of experimental data for the adsorption of methyl orange from aqueous solution using a low cost activated carbon prepared from *Prosopis juliflora*. *Polish Journal of Chemical Technology*, 15(2):29-39

[36] Akalin, H.A. Hiçsönmez, Ü.and Yilmaz, H. (2017). Removal of Cesium from Aqueous Solution by Adsorption onto Sivas-Yildizeli (Türkiye) Vermiculite: Equilibrium, Kinetic and Thermodynamic Studies. *Journal of the Turkish chemical society section A JOTCSA* 5(1): 85-116